

Two-Dimensional Transition Metal Carbides

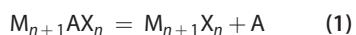
Michael Naguib,^{†,*} Olha Mashtalir,^{†,*} Joshua Carle,[†] Volker Presser,^{†,*} Jun Lu,[§] Lars Hultman,[§] Yury Gogotsi,^{†,*} and Michel W. Barsoum^{†,*}

[†]Department of Materials Science and Engineering and [‡]A.J. Drexel Nanotechnology Institute, Drexel University, Philadelphia, Pennsylvania 19104, United States, and [§]Department of Physics, IFM Linköping University, Linköping 58183, Sweden

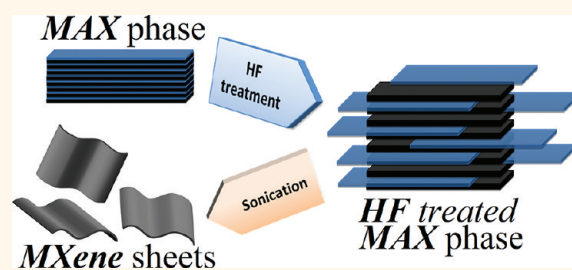
Two-dimensional (2-D) materials, such as graphene, are known to have unique properties^{1–4} that, in turn, can potentially lead to some promising applications.^{5–12} Over the years, other 2-D materials with different chemistries have been synthesized by exfoliation of layered 3-D precursors such as boron nitride,¹³ metal chalcogenides (e.g., MoS₂,^{14,15} WS₂^{16,17}), oxides, and hydroxides.^{18–20} In most, if not all, of these cases, the initial bonding between the layers was relatively weak, making the structure amenable to exfoliation.

As far as we are aware, and until our recent work,²¹ the exfoliation of layered solids with strong primary bonds had not been reported. Very recently, we reported on the exfoliation of the layered transition metal carbide, Ti₃AlC₂.²¹ A schematic of the exfoliation process is shown in Figure 1. We note that Ti₃AlC₂ is a member of a large family of layered hexagonal (space group *P6₃/mmc*) ternary metal carbides and nitrides referred to as the MAX phases. The term MAX phases reflects the chemical composition: M_{*n*+1}AX_{*n*}, where *n* = 1, 2, or 3 (M₂AX, M₃AX₂, or M₄AX₃, etc.), “M” is an early transition metal, “A” is an A group (mostly groups 13 and 14) element, and “X” is C and/or N.²² These solids combine unusual and sometimes unique properties, as they are easily machinable and, in addition to being highly damage tolerant, extremely thermal shock resistant.²³ Some MAX phases, most notably, Ti₃AlC₂, are also quite oxidation resistant, especially when compared to their chemically related binary carbides.²⁴

In general, the MAX phases are chemically quite stable, but the A layers are chemically more reactive because they are relatively weakly bonded when compared to the M–X bonds. At high temperatures, the MAX phases partially decompose according to the following reaction.²⁵



ABSTRACT



Herein we report on the synthesis of two-dimensional transition metal carbides and carbonitrides by immersing select MAX phase powders in hydrofluoric acid, HF. The MAX phases represent a large (>60 members) family of ternary, layered, machinable transition metal carbides, nitrides, and carbonitrides. Herein we present evidence for the exfoliation of the following MAX phases: Ti₂AlC, Ta₄AlC₃, (Ti_{0.5}Nb_{0.5})₂AlC, (V_{0.5}Cr_{0.5})₃AlC₂, and Ti₃AlCN by the simple immersion of their powders, at room temperature, in HF of varying concentrations for times varying between 10 and 72 h followed by sonication. The removal of the “A” group layer from the MAX phases results in 2-D layers that we are labeling MXenes to denote the loss of the A element and emphasize their structural similarities with graphene. The sheet resistances of the MXenes were found to be comparable to multilayer graphene. Contact angle measurements with water on pressed MXene surfaces showed hydrophilic behavior.

KEYWORDS: MXene · two-dimensional materials · carbides · carbonitrides · exfoliation

Such high decomposition temperatures, however, induce recrystallization and the M_{*n*+1}X_{*n*} layers turn into nonlayered, bulk 3-D cubic carbides and/or nitrides with rock-salt structures with some ordering of the vacancies on the X sites.^{25–27}

It is important to note that the bonding in the MAX phases is a combination of metallic, covalent, and ionic bonding, and the bonding strength is, in most cases, quite strong.²⁵ Many of these compounds, especially the Al-containing ones, were fabricated at temperatures as high as 1600 °C. For example, the Ti₃AlC₂ powders tested in our previous work were synthesized at 1350 °C,²¹ and bulk Ti₂AlC samples are hot pressed at 1600 °C.²⁸

* Address correspondence to gogotsi@drexel.edu, barsoumw@drexel.edu.

Received for review October 27, 2011 and accepted January 26, 2012.

Published online January 26, 2012
10.1021/nn204153h

© 2012 American Chemical Society

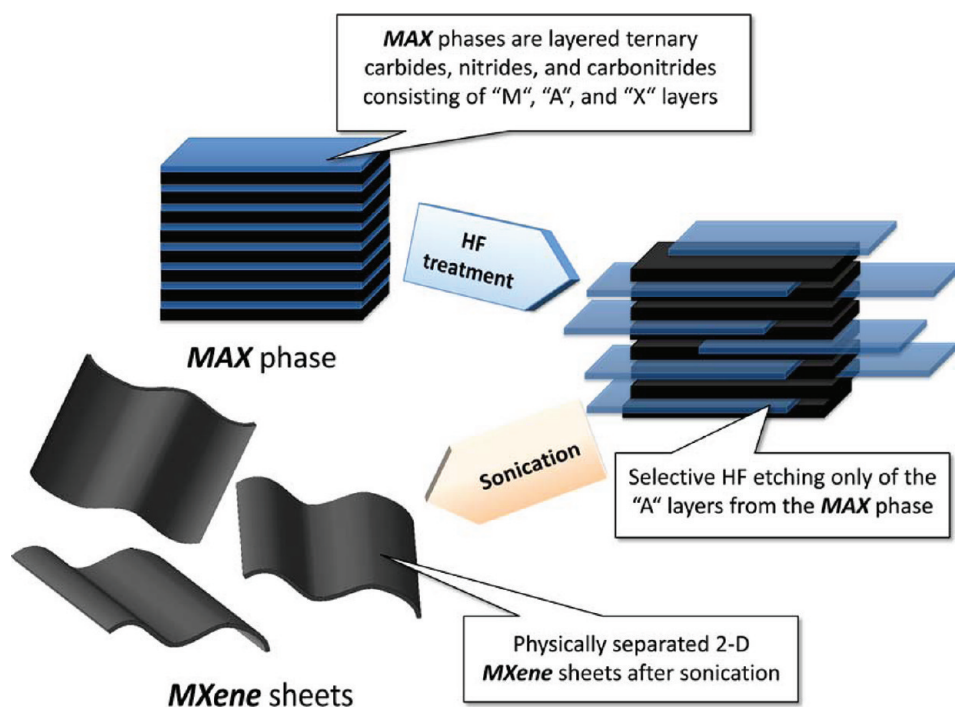
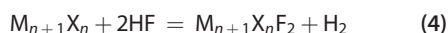
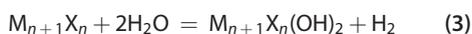
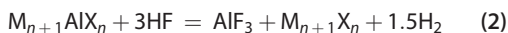


Figure 1. Schematic for the exfoliation process of MAX phases and formation of MXenes.

Our first attempt to exfoliate MAX phases was carried out by immersing Ti_3AlC_2 powders in 50% hydrofluoric acid, HF, at room temperature for 2 h. This procedure resulted in the selective etching of the aluminum, Al, layers and their replacement by hydroxyl, OH, and fluorine, F, surface groups. Besides nanosheets, we also observed scrolls, nanotubes, and multilayers of Ti_3C_2 after sonication. In that work, and given that over 60 MAX phases are known to exist, we speculated that Ti_3C_2 could very well represent a member of a much larger family of 2-D transition metal carbides and/or nitrides. To emphasize their similarity to graphene, we proposed to label these 2-D solids "MXenes".

The purpose of this paper is to show that indeed it is possible to exfoliate a number of chemically quite diverse, Al-containing MAX phases. In all cases, the operative reactions are presumed to be



The following MAX phases were chosen for study: Ti_2AlC , Ta_4AlC_3 , Ti_3AlCN , $(\text{V}_{0.5}, \text{Cr}_{0.5})_3\text{AlC}_2$, and $(\text{Ti}_{0.5}, \text{Nb}_{0.5})_2\text{AlC}$, henceforth referred to as TiNbAlC. The first two were chosen to show that it is possible to exfoliate both M_2AX (211) and M_4AX_3 (413) phases, in addition to the already exfoliated M_3AX_2 (312) phase. The $(\text{V}_{0.5}, \text{Cr}_{0.5})_3\text{AlC}_2$ and TiNbAlC compositions were chosen to show that the M element needs neither to be confined to Ti nor be a single element; Ti_3AlCN was chosen to

show that the X element need not be confined to C but can also be a mixture of C and N.

RESULTS AND DISCUSSION

The HF treatment process yield, Y , was obtained by measuring the initial powder weight before HF treatment (W_i) and the weight, W_f , after HF treatment (i.e., after several iterations of washing and subsequent drying). Y was then calculated to be the ratio $W_f/W_i \times 100\%$. We note that the values reported in Table 1 are, thus, most likely lower than the actual synthesis yields because some powder is inevitably lost in the washing steps.

The structures before and after HF treatment were characterized by X-ray diffraction (XRD) and scanning electron microscopy (SEM). The MXene sheets were investigated using transmission electron microscopy (TEM) and optical microscopy (OM). The resistivity and contact angle measurements were carried out on cold pressed discs (shown in Figure 2) of HF-treated powders.

The starting Ti_2AlC powders (Figure 3A-a) contain small amounts of Ti_3AlC_2 and TiC as secondary phases, which were estimated to be <5 wt % by Rietveld analysis. Figure 3A-b shows the XRD pattern of the HF-treated powders. Figures 3A-c and A-d show, respectively, the diffractograms of the HF-treated and as received powders after cold pressing. Figure 3B-a–d shows the corresponding results for Ta_4AlC_3 and Figure 3C those for TiNbAlC. The results for $(\text{V}_{0.5}, \text{Cr}_{0.5})_3\text{AlC}_2$ are shown only as an inset in Figure 3C for brevity's sake and because the exfoliation protocol did not

TABLE 1. List of MAX Phases Exfoliated in This Work and Exfoliation Process Parameters^a

compound	HF conc. (%)	time (h)	c lattice constant (nm)		domain size (nm)	yield (wt %)	associated figures
			before HF	after HF			
Ti ₂ AlC	10	10	1.36	1.504	6	60	2A, 3A, and 4C
Ta ₄ AlC ₃	50	72	2.408	3.034	38	90	2B, 3B, 4D, 5D, 6A–D, and 8A
				2.843	18		
TiNbAlC	50	28	1.379	1.488	5	80	2C, 3C, 4E, 5C and 7A,B
(V _{0.5} Cr _{0.5}) ₃ AlC ₂	50	69	1.773	2.426	28	NA	inset 3C and 7C,D
Ti ₃ AlCN	30	18	1.841	2.228	7	80	2D, 3D, 4F, 5B, and 8B
Ti ₃ AlC ₂	50	2	1.842	2.051	11	100	4A,B

^a The particle size for all MAX phases was <35 μm prior to exfoliation. The effects of HF treatment on the c lattice constant and the average domain size along [0001] deduced from the FWHM and the Scherrer formula are listed. The penultimate column shows the estimated process yields. The last column lists the figures associated with each compound.

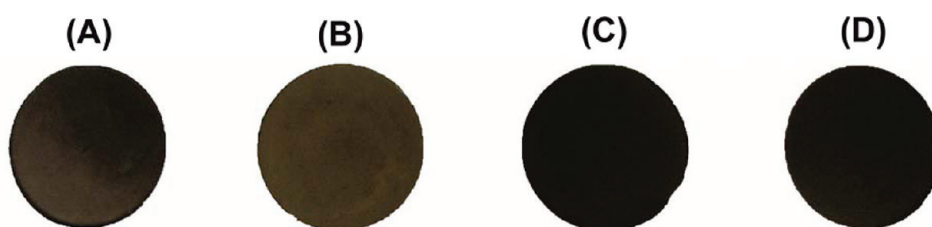


Figure 2. Photograph of cold-pressed, free-standing discs with diameters of 25 mm of (A) Ti₂C, (B) Ta₄C₃, (C) TiNbC, and (D) Ti₃CN_x.

result in the total conversion of the compound to its corresponding MXene. The XRD results for Ti₃AlCN, before and after HF treatment, are shown in Figure 3D.

A perusal of the XRD results depicted in Figure 3 clearly demonstrates a drastic loss in crystallinity and structural order after exfoliation. Note that, in several cases, small amounts of MX phases (with a rock-salt crystal structure) were present in the initial powders. These do *not* react and the full width at half-maximum, FWHM, of their peaks remains unchanged after HF treatment. In sharp contradistinction, the (0002) peaks of the treated powders are all shifted to lower angles corresponding to higher c parameters. The same peaks also broaden considerably. Using the Scherrer formula,²⁹ the domain size along [0001] was found to shrink considerably after the HF treatment (see column 6 in Table 1). The values correspond to about 3 unit cells in case of the M₂AX phases and to about 15 in case of Ta₄AlC₃.

Even after 65 h in a 50% HF solution, the (V_{0.5}, Cr_{0.5})₃AlC₂ powders were not fully reacted. This is best seen in the inset in Figure 3C, in which there are two distinct peaks after HF treatment: one around 9.9° 2 θ that corresponds to the (0002) peak of unreacted (V_{0.5}, Cr_{0.5})₃AlC₂; the other a broader peak at 7.3° 2 θ due to the exfoliated (V_{0.5}, Cr_{0.5})₃AlC₂. Note that the latter peak appeared only after cold pressing of the HF-treated powders.

The yields listed in column 7 in Table 1 are quite high, indicating that for the conditions reported in Table 1 little dissolution occurs in the HF solutions. We note in passing that the main challenge of this work was to identify the combination of acid strength and

immersion times that were not too mild as to not etch the Al or too aggressive as to dissolve the MAX/MXene powders or form ternary fluorides. For example, non-aqueous 100% HF treatment of Ti₂AlC results in the formation of a nanocrystalline ternary titanium aluminum fluoride, Ti₂AlF₉.³⁰ When Ti₂AlC powders were placed in 50% HF solution for 2 h, they completely dissolved, and while it is obvious that the HF treatment resulted in similar end products, there are subtle differences between each of the MXene phases produced. Consequently, each will be discussed separately.

Ti₂AlC. After etching the Al out of this structure (10% HF for 10 h), the degree of order as measured by XRD clearly decreased (Figure 3A-b). It is only after cold pressing (Figure 3A-c) that the Ti₂C layers were forced to restack/reorient in their preferred orientation. When comparing the XRD pattern of the cold-pressed Ti₂AlC powders—before and after treatment—it is clear that the (0002) peak, which was initially at $\approx 13^\circ$ 2 θ , broadened and shifted to a lower angle after treatment; that is, it shifted to larger d spacings. Small peaks of exfoliated Ti₃AlC₂, initially present as a secondary phase in the as-received Ti₂AlC powder, identical to those reported earlier were also observed.²¹

The SEM image of Ti₂AlC after the HF treatment (Figure 4C) confirms successful exfoliation of individual particles, which is similar to what was reported for exfoliated graphite^{31–33} or Ti₃AlC₂ (Figure 4B), where the layers are clearly separated from each other compared to the unreacted powder (Figure 4A). Sonication of the treated powders resulted in the separation of

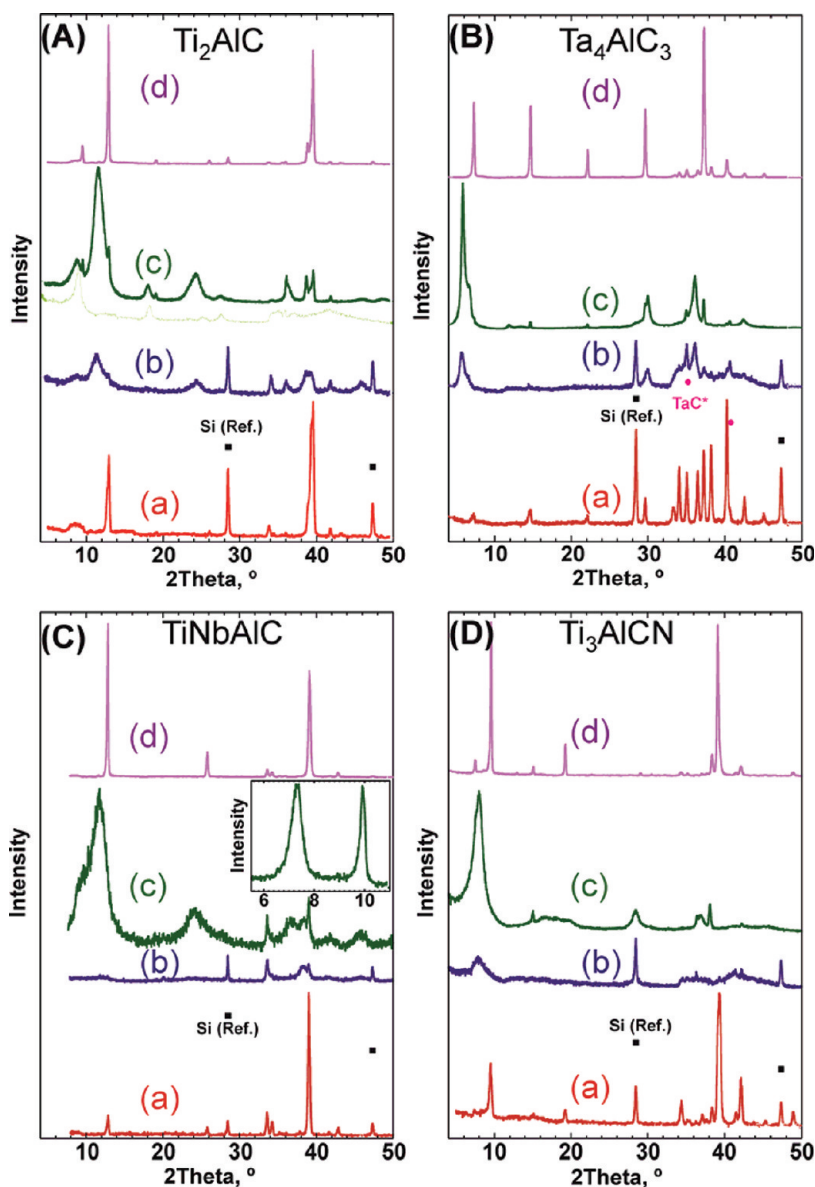


Figure 3. XRD patterns before and after HF treatment at room temperature for (A) Ti_2AlC (10% HF for 10 h), (B) Ta_4AlC_3 (50% HF, 72 h), (C) TiNbAlC (50% HF 28 h), and the inset is the XRD for $(\text{V}_{0.5}\text{Cr}_{0.5})_3\text{AlC}_2$ (50% HF 65 h) and cold-pressed zoomed-in on the (0002) peak, and (D) Ti_3AlCN (30% HF 18 h). The diffractograms of each panel represent, from bottom to top, (a) MAX phase before HF treatment, (b) MAX phase after HF treatment, (c) cold-pressed MXene after HF treatment of MAX phases, and (d) MAX phase cold-pressed prior to HF treatment.

2-D sheets, and energy-dispersive X-ray (EDX) microanalysis after exfoliation showed the Ti/C/F/O \approx atomic ratios to be 39:19:20:22, respectively. The absence of Al suggests the following reaction:



This reaction is presumably followed by reactions 3 and 4 and results in 2-D layers of Ti_2C with hydroxyl and/or F surface groups; the latter explains the presence of O and F after treatment. Note that whenever the MAX powders were immersed in the HF solution, bubbles, presumably H_2 , were observed.

Ta_4AlC_3 . After HF treatment (50% HF for 72 h), the XRD (Figure 3B-c) and electron microscopy (Figure 4D)

document the successful exfoliation of Ta_4AlC_3 . We note that the (0002) XRD peak after treatment has a clearly visible shoulder. Peak deconvolution yields a first reflection ascribed to a c parameter of ≈ 3.034 nm (domain size of ≈ 38 nm; *i.e.*, about 12 unit cells along [0001]) and a second peak corresponding to a c parameter of 2.843 nm (domain size of ≈ 18 nm; *i.e.*, about 6 unit cells along [0001]). The reason for the shoulder is unclear at this time, and one possible explanation is that the untreated powders contained two polymorphs of Ta_4AlC_3 .³⁴ This comment notwithstanding, more work is needed to understand the origin of the observed shoulder.

The TEM micrographs of HF treated Ta_4AlC_3 are shown in Figure 5D. Figure 6A shows a higher

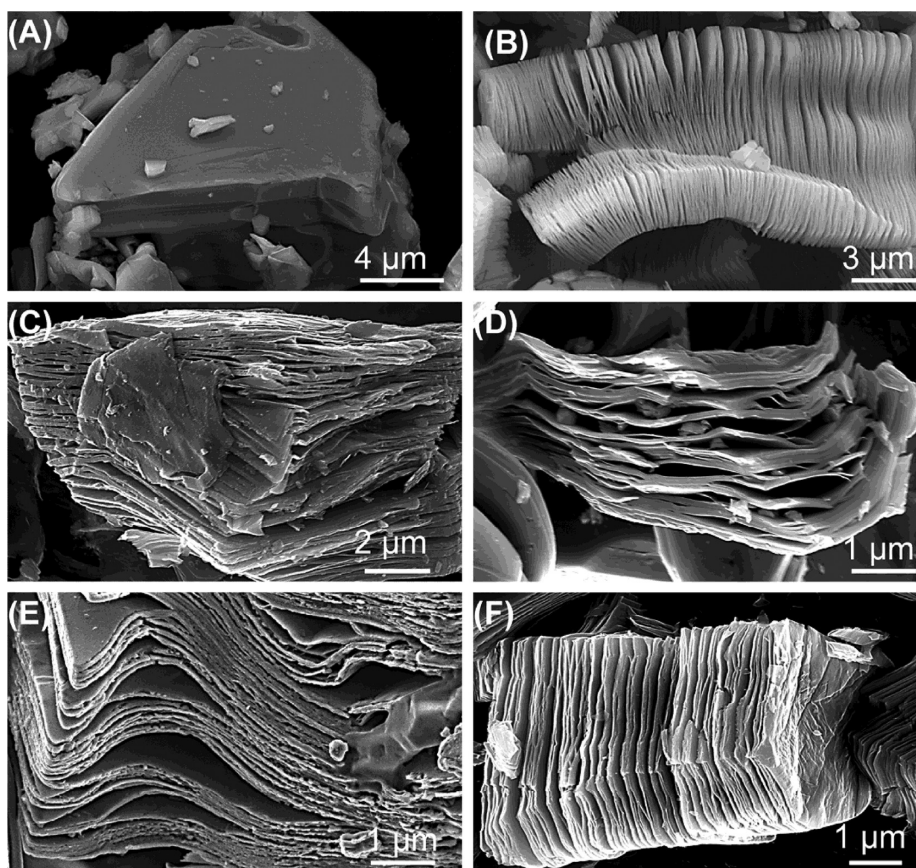


Figure 4. Secondary electron SEM micrographs for (A) Ti_3AlC_2 particle before treatment, which is typical of unreacted MAX phases, (B) Ti_3AlC_2 after HF treatment, (C) Ti_2AlC after HF treatment, (D) Ta_4AlC_3 after HF treatment, (E) TiNbAlC after HF treatment, and (F) Ti_3AlCN after HF treatment. In (B–F), the exfoliation is obvious.

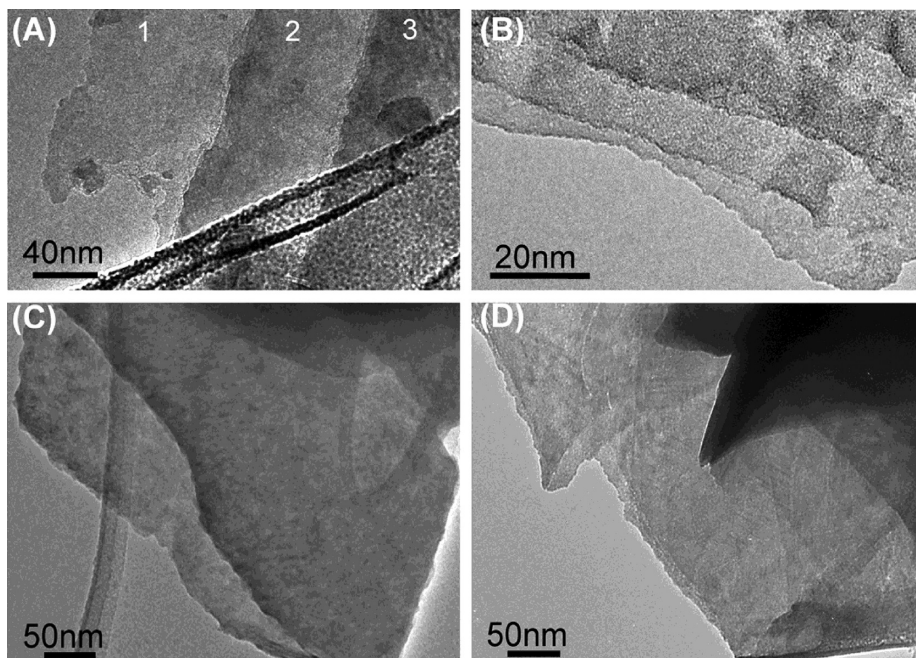


Figure 5. TEM images for (A) Ti_3C_2 layers formed after HF treatment of Ti_3AlC_2 at room temperature for 22 h assuming a single sheet (monolayer) is the most transparent part of the sample, (B) similar layers of Ti_3CN_x , exfoliated from Ti_3AlCN by HF treatment, (C) TiNbAlC after HF treatment, and (D) Ta_4AlC_3 after HF treatment. Numbers show an increasing number of layers from the thinnest and most transparent to electrons (1, presumably a monolayer) to 2, 3, or more layers.

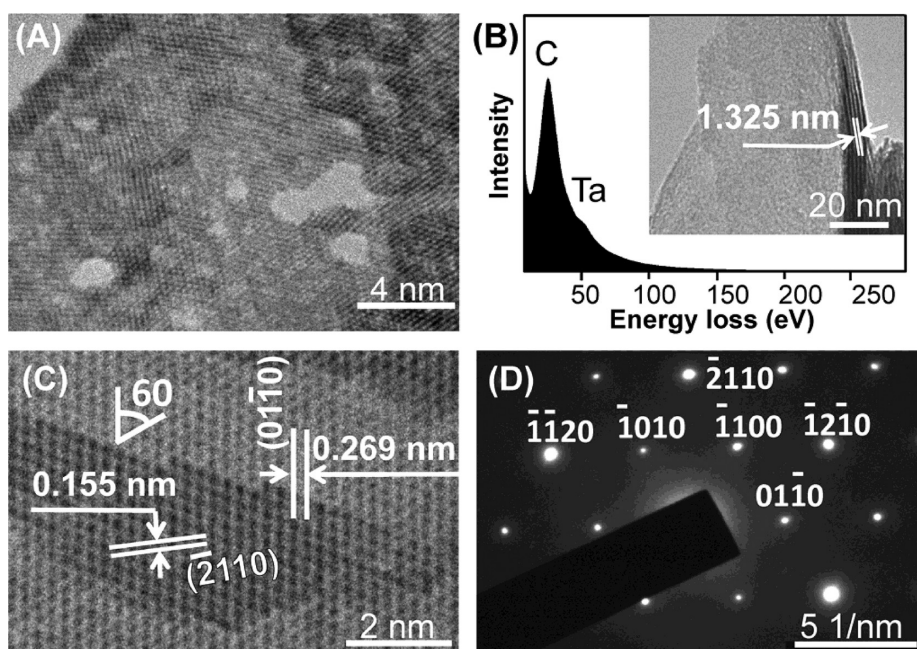


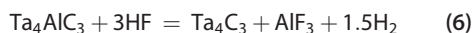
Figure 6. Electron microscopy analysis of Ta_4AlC_3 after HF treatment (A) TEM image, (B) EELS and inset showing a low-magnification TEM image, (C) HRTEM of multilayer MXene, and (D) SAED.

magnification high-resolution transmission electron microscope (HRTEM) image of a Ta_4C_3 layer with some nanometer sized holes. Similar atomic defects were reported in functionalized graphene.³⁵ The latter can act as nucleation sites for metal oxides which are useful in many applications.^{36,37} The electron energy loss spectra (EELS) (Figure 6B) confirm the presence of C, Ta, O (not shown), some F (not shown) and the absence of Al, confirming that it was etched out from the structure.

HRTEM and selected area electron diffraction (SAED) (Figure 6C,D), however, show that the crystallinity of the basal planes of the MAX phases is preserved. These images confirm the hexagonal structure of the Ta_4C_3 layers. Measurements of the d spacings shown in the figure resulted in 0.269 and 0.155 nm for the $(01\bar{1}0)$ and $(\bar{2}110)$ lattice planes, respectively. When these values are used to calculate the a lattice parameter, the value obtained, 0.31 nm, is in excellent agreement with that of the a parameter of the nonexfoliated Ta_4AlC_3 MAX phase, viz. 0.311 nm.³⁸ It is thus reasonable to conclude that the MAX crystal structure of the basal planes is maintained in the MXenes.

As shown in Figure 8A, the Ta_4C_3 layers are not just electronically transparent but also optically transparent under an OM in transmittance mode.

After exfoliation, EDX showed the Ta/C/F/O atomic ratios to be 40:39:7:14, respectively. The absence of Al, together with the other evidence, suggests the following reaction:



This reaction is presumably followed by reactions 3 and 4.

TiNbAlC and $(\text{V}_{0.5}, \text{Cr}_{0.5})_3\text{AlC}_2$. The XRD patterns for TiNbAlC, before and after HF treatment (Figure 3C), show that the intensity of the TiNbAlC peaks decreased significantly after HF treatment (considering that 10 wt % Si was used as an internal reference) and a new broad peak at $\approx 11.8^\circ 2\theta$ appeared after cold pressing (Figure 3C-c), similar to what was reported previously.²¹ Here again a shoulder at a larger d spacing compared to the main peak is observed. The latter is most likely due to some exfoliated $(\text{Ti}_{0.5}, \text{Nb}_{0.5})_3\text{AlC}_2$ that was present as a second phase in the starting powder, similar to what was discussed above and shown in Figure 3A-c.

SEM micrographs (Figure 4E) clearly show exfoliated TiNbAlC particles. TEM micrographs, after sonication (Figure 5C), show thin sheets composed of Ti, Nb, C, O, and F in an atomic ratio that EDX shows to be 14:16:23:34:13, respectively. TEM micrographs (Figure 5C) are noteworthy in that the carbon grid is visible through TiNbC layers. Given the fact that Ti and Nb are heavy elements, this implies that the layers must be quite thin indeed.

HRTEM of a TiNbC layer, shown in Figure 7A, and its corresponding SAED (inset) again show hexagonal symmetry. At 0.2606 nm, the perpendicular separation of the $(10\bar{1}0)$ lattice planes results in an a lattice constant of 0.301 nm, a value that is in good agreement with what was reported for TiNbAlC,³⁹ viz. 0.308 nm. Figure 7B shows EELS for TiNbAlC after HF treatment and confirms the presence of Ti, Nb, C, F (not shown), and O, but no Al.

As noted above, the $(\text{V}_{0.5}, \text{Cr}_{0.5})_3\text{AlC}_2$ powders did not undergo complete exfoliation as indicated by the presence of two distinct peaks in the inset of Figure 3C.

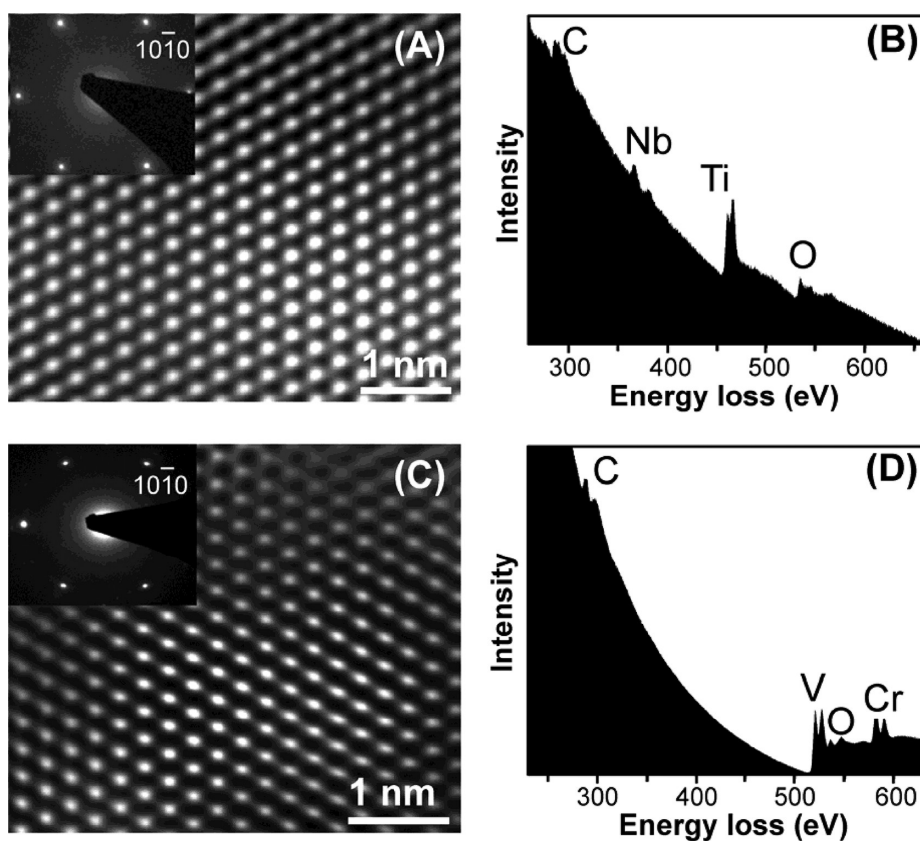


Figure 7. (A) HRTEM for TiNbAlC after HF treatment and the inset (top left) showing SAED, (B) corresponding EELS spectrum for HF-treated TiNbAlC, (C) HRTEM for $(V_{0.5}Cr_{0.5})_3AlC_2$ after HF treatment and the inset (top left) is showing SAED, and (D) corresponding EELS results for HF-treated $(V_{0.5}Cr_{0.5})_3AlC_2$.

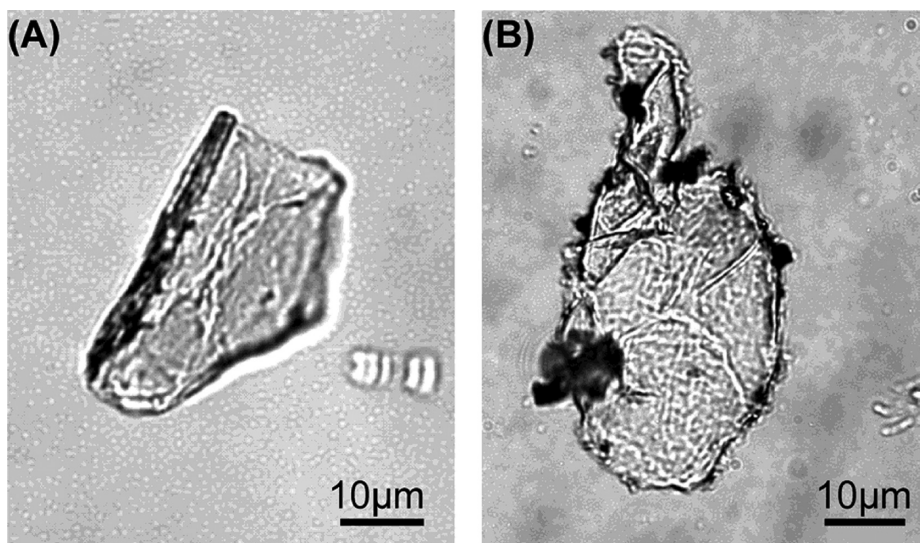


Figure 8. Transmitted light micrographs of exfoliated flakes of (A) Ta_4C_3 and (B) Ti_3CN_x .

All other observations are consistent in that at least a fraction was exfoliated. Note that by varying the concentration and/or reaction times, fully exfoliated $(V_{0.5}Cr_{0.5})_3C_2$ 2-D layers should be readily obtainable. HRTEM for an exfoliated layer of $(V_{0.5}Cr_{0.5})_3C_2$ after HF treatment (Figure 7C) and its corresponding SAED (inset) confirm the same hexagonal crystal structure as was shown for all previous exfoliated phases. At

0.286 nm, the a lattice parameter, calculated from the $(01\bar{1}0)$ reflections, is in excellent agreement with that of $(V_{0.5}Cr_{0.5})_3AlC_2$, viz. 0.289 nm.⁴⁰ Figure 7D shows EELS for $(V_{0.5}Cr_{0.5})_3AlC_2$ after HF treatment and confirms the presence of V, Cr, C, F (not shown), and O but no Al.

Ti₃AlCN. HF treatment (30% HF, 18 h) of the Ti_3AlCN powders resulted in complete exfoliation as evidenced

TABLE 2. Resistivity and Contact Angle of Water on Cold-Pressed Free-Standing Discs for Different Exfoliated Phases and Their Densities

property of MXene	Ti ₂ C	TiNbC	Ti ₃ CN _x	Ta ₄ C ₃	Ti ₃ C ₂
resistivity, Ω/□	339	171	125	104	22
resistivity, Ω m	0.068	0.052	0.037	0.021	0.005
contact angle, deg	32	31	27	41	34
density of the cold pressed discs, ^a g/cm ³ (% of theoretical)	2.91 (62%)	3.23 (52%)	2.95 (64%)	6.82 (53%)	3.12 (60%)

^aThe densities were estimated from the dimensions and weights of the cold-pressed discs. Number in parentheses is relative theoretical density assuming OH termination of MXene surfaces and the *c* parameters listed in Table 1.

by XRD (Figure 3D). EDX showed Ti, C, O, and F, which implies that the 2-D Ti₃CN_x layers are terminated with OH and/or F surface groups. SEM (Figure 4F), TEM (Figure 5B), and optical micrographs (Figure 8B) show evidence for exfoliated Ti₃CN_x layers that are transparent to both the electron beam and visible light. While no N was detected by EELS, the presence of nitrogen in exfoliated samples was confirmed by other methods. This may be because the N/C ratio is lower than the starting ratio (*i.e.*, *x* < 1.0) or due to the presence of both carbide and carbonitride particles in the as-received MAX phase.

A picture of the cold-pressed discs of the different MXene compositions is shown in Figure 2. Their densities (Table 2) varied between 2.91 g/cm³ for Ti₂C to 6.82 g/cm³ for Ta₄C₃. If one assumes the *c* lattice parameters listed in Table 1 and OH terminated surfaces of MXene sheets, then it is possible to calculate the theoretical densities. The last row in Table 2 lists the measured densities of the pressed discs. The numbers in parentheses list the % of theoretical densities that range from 50 to ≈65%.

The sheet resistivity and resistivities of the various MXene discs are also shown in Table 2. Generally, these values are comparable to multilayer graphene reported by Li *et al.*⁴¹ and Blake *et al.*⁴² The resistivity values are higher than the MAX phases before treatment (<10 Ω/□) presumably because of the replacement of the A layers with OH and/or F. When it is assumed that surface groups are similar in all of the exfoliated MAX phases, the difference in the resistivity between the different phases can be partially explained by the different number of atomic layers (3, 5, and 7 for M₂X, M₃X₂, and M₄X₃ phases, respectively). It is important to note that the resistivity values reported in Table 2 should be significantly higher than single MXene sheets because of the method by which the resistivity was measured. For example, the resistivity of bulk sintered Ti₃AlC₂ is 0.39 μΩ m.²⁵ When Ti₃AlC₂ powders were cold-pressed at 1 GP, their resistivity increased to 1200 μΩ m, a, roughly, 3000 time increase.

Contact angle measurement results for water droplets on the cold-pressed discs of exfoliated phases are also listed in Table 2. These values are lower than those of the corresponding MAX phases—that were also measured in this work on cold-pressed samples, which

were around 60°. The reduction in contact angle can be explained by the presence of OH surface groups after the HF treatment. In contradistinction, graphene can be transformed from superhydrophobic to superhydrophilic by altering the surface groups.⁴³ The hydrophilicity of the MXenes would be an advantage when using aqueous electrolytes in energy storage devices or dispersing in water and alcohols for further processing.

Lastly, it is important to note that the only other transition metal elements that form MAX phases not included above are Hf, Mo, and Zr. These elements do not form MAX phases with Al, the focus of this study. On the basis of our work, however, we believe that it is only a matter of time before 2-D Hf₂C, Mo₂C, and Zr₂C are also synthesized. The same applies to the following pure nitride phases: Ti₄N₃, Ti₂N, Cr₂N, Zr₂N, and Hf₂N although at this time the stability of N-containing MXenes is lower than their carbide counterparts. In short, we are looking at a large number of 2-D early transition metal carbides, nitrides, and/or carbonitrides. The latter is especially true when solid solutions on the M and X sites, or both, are factored in.

In particular, tailoring surface functional groups of MXene 2-D layers presents itself as another variable for tuning their surface (*e.g.*, wetting) and electrical (*e.g.*, band gap, conductivity)²¹ and electrochemical (*e.g.*, pseudocapacitance) properties, like in graphene.⁴⁴ With such a large variety of possible chemistries, it is reasonable to assume that at least some of them will have unique enough properties to lead to applications in multiple fields and technologies, such as catalysis, energy storage/pseudocapacitors, and Li-ion batteries as we have just shown for Ti₂C,⁴⁵ as well as potential reinforcements in polymers. The resulting 2-D layers are stiff when pulled parallel to the basal planes, quite conductive (Table 2),²¹ and should be more oxidation resistant than graphene because the oxide/hydroxide layer present on their surfaces may offer protection.

CONCLUSIONS

Recently, we showed that when Ti₃AlC₂ powders were immersed in HF, the Al layers were selectively extracted to yield 2-D Ti₃C₂ layers terminated with OH and/F surface groups. Herein we significantly expand this nascent large family of 2-D, M_{*n*+1}X_{*n*} layers to Ti₂C,

Ta₄C₃, TiNbC, (V_{0.5}Cr_{0.5})₃C₂, and Ti₃CN_x, where $x < 1$. The exfoliation occurs at room temperature, and the yields are quite high. It is thus obvious that we are dealing with a large family of materials that we are

labeling MXene to emphasize their 2-D nature and their similarities to graphene. Cold-pressed discs of different MXene sheets showed good electrical conductivities and hydrophilic behavior.

MATERIALS AND METHODS

Synthesis of MAX Phases and Exfoliation into MXenes. Prereacted Ti₂AlC powders were commercially obtained (3-ONE-2, Voorhees, NJ, >92 wt % purity; particle size <44 μm, *i.e.*, –325 mesh).

The Ta₄AlC₃ powders were made by mixing elemental tantalum, Ta (Alfa Aesar, Ward Hill, USA, 99.97 wt % purity; –325 mesh), aluminum, Al (Alfa Aesar, Ward Hill, USA, 99.5 wt % purity; –325 mesh), and graphite, C (Alfa Aesar, Ward Hill, USA, 99 wt % purity; particle size <48 μm, *i.e.*, –300 mesh) powders in a 4:1.75:3 molar ratio. The powders were ball-milled for 12 h and cold-pressed into cylindrical discs, (25 mm diameter and roughly 10 mm high), under pressure of 500 MPa. The discs were placed in a tube furnace, under flowing argon, Ar, and heated at 10 °C/min to 1500 °C for 1 h. The resulting ≈70% dense discs were then milled using a titanium-nitride-coated milling bit to obtain powders for further study. In all cases, the milled powder was sieved through a –400 mesh screen such that the initial particle size was <35 μm.

The TiNbAlC powders were made by mixing elemental titanium, Ti (Alfa Aesar, Ward Hill, USA, 99.5 wt % purity; –325 mesh), niobium, Nb (Atlantic Equipment Engineers, Bergenfield, USA, 99.8 wt % purity; –325 mesh), and the same Al and C used above, in the molar ratio of 1:1:1.2:1, respectively, in a ball mill for 12 h. The powders were then heated at the rate of 10 °C/min in a tube furnace to 1500 °C for 1 h under flowing Ar. After cooling to room temperature, powders were processed as described above.

The (V_{0.5}Cr_{0.5})₃AlC₂ powders were made by mixing elemental vanadium, V (Alfa Aesar, Ward Hill, USA, 99 wt % purity; –325 mesh), chromium, Cr (Alfa Aesar, Ward Hill, USA, 99 wt % purity; –325 mesh), and the same Al and C used above, in the molar ratio of 1.5:1.5:1.2:2, respectively, in a ball mill for 12 h. The mixed powders were then heated 10 °C/min to 1550 °C and held at that temperature in a tube furnace under flowing Ar for 2 h. After cooling to room temperature, powders were produced by milling as above.

The Ti₃AlCN powders were made by mixing elemental Ti (Alfa Aesar, Ward Hill, USA, 99.5 wt % purity; –325 mesh), aluminum nitride, AlN (Sigma Aldrich, St. Louis, USA, 99 wt % purity; particle size <10 μm), and the graphite, described above, in the 3:1:1 molar ratio, respectively, for 12 h in a ball mill. The mixture was then heated in a tube furnace at 10 °C/min to 1500 °C and held at that temperature under flowing Ar for 2 h. After cooling to room temperature, powder was produced by crushing the lightly sintered powder compact in a mortar and pestle.

Each of the aforementioned MAX phase sieved powders was immersed at room temperature in HF (Fisher Scientific, Fair Lawn, NJ) solutions of varying potency for various times. Table 1 summarizes the times and concentrations used.

In all cases, the resulting suspension was then washed several times using deionized water and centrifuged to separate the powders from the supernatant.

Characterization. X-ray diffraction (XRD) patterns were obtained with a powder diffractometer (Siemens D500, Germany) using Cu Kα radiation and a step scan of 0.02° and 1 s per step. Si powder was added to some samples as an internal standard to calibrate the diffraction angles and the instrumental peak broadening.

To accentuate that HF treatment mostly affects the *c* parameter and given that both MAX and MXenes are easily oriented, in all cases, we not only compared the diffractograms of the as-fabricated and HF-treated powders deposited on glass slides but more importantly we also compared diffractograms of discs that were produced by cold pressing the powders at loads

corresponding to 1 GPa. In all cases, the cold pressing resulted in thin, free-standing discs shown in Figure 2.

A scanning electron microscope, SEM (Zeiss Supra 50VP, Germany), was used to obtain high-magnification images of the treated powders and conduct elemental analysis *via* energy-dispersive X-ray (EDX) spectroscopy. After sonication, the 2-D sheets were investigated by transmission electron microscopy, TEM (JEOL JEM-2100, Japan), with an accelerating voltage of 200 kV. Electron energy loss spectroscopies (EELS) were obtained using FEI Tecnai G2 TF 20 UT field emission gun TEM operated at 200 kV with 0.19 nm point resolution and 0.7 eV energy resolution for EELS. The TEM samples were prepared by suspending the powders in isopropyl alcohol and placing a drop of the latter on a lacey carbon coated 200 mesh Cu grid.

After HF treatment and sonication of the resultant powder in isopropyl alcohol, a droplet from the suspension was placed on a glass slide and investigated using an optical microscope, OM (S8AP0: Leica Microsystems Inc., Bannockburn, IL, USA) in transmitted light mode.

To measure the sheet resistances and the contact angle, MXene discs (25 mm in diameter, 300 μm thick) were cold-pressed from the reacted powders. The latter were placed in a die and cold-pressed to a load corresponding to a stress of 1 GPa (Figure 2).

The surface or sheet resistances of cold-pressed, free-standing MXene discs (Figure 2) were measured using a four-probe technique (Cascade Probe Station CPS-1303-24 with 4-point probe head Alessi C45-57, Cascade Microtech, Inc., Beaverton, USA).

Contact angle measurements of deionized water were also performed at room temperature using the sessile drop technique. Ten microliter water drops were placed on the surfaces of cold-pressed MXene discs. The contact angles were measured from photographs taken with a CCD camera yielding an accuracy of approximately ±3°.

Conflict of Interest: The authors declare no competing financial interest.

Acknowledgment. This work was supported by the Assistant Secretary for Energy Efficiency and Renewable Energy, Office of Vehicle Technologies of the U.S. Department of Energy under Contract No. DE-AC02-05CH11231, Subcontract 6951370 under the Batteries for Advanced Transportation Technologies (BATT) Program. Also supported by the Commonwealth of Pennsylvania's Ben Franklin Technology Development Authority through the Ben Franklin Technology Partners of Southeastern Pennsylvania. V.P. acknowledges financial support by the Alexander von Humboldt Foundation. Use of the equipment of the Centralized Research Facility (Drexel University) is acknowledged.

REFERENCES AND NOTES

- Novoselov, K. S.; Geim, A. K.; Morozov, S. V.; Jiang, D.; Zhang, Y.; Dubonos, S. V.; Grigorieva, I. V.; Firsov, A. A. Electric Field Effect in Atomically Thin Carbon Films. *Science* **2004**, *306*, 666–669.
- Rao, C. N. R.; Subrahmanyam, K. S.; Matte, H. S. S. R.; Abdulhakeem, B.; Govindaraj, A.; Das, B.; Kumar, P.; Ghosh, A.; Late, D. J. A Study of the Synthetic Methods and Properties of Graphenes. *Sci. Technol. Adv. Mater.* **2010**, *11*, 054502.
- Sasaki, T. Fabrication of Nanostructured Functional Materials Using Exfoliated Nanosheets as a Building Block. *J. Ceram. Soc. Jpn.* **2007**, *115*, 9–16.
- Pisana, S.; Braganca, P. M.; Marinero, E. E.; Gurney, B. A. Tunable Nanoscale Graphene Magnetometers. *Nano Lett.* **2009**, *10*, 341–346.

5. Stoller, M. D.; Park, S.; Zhu, Y.; An, J.; Ruoff, R. S. Graphene-Based Ultracapacitors. *Nano Lett.* **2008**, *8*, 3498–3502.
6. Schwierz, F. Graphene Transistors. *Nat. Nanotechnol.* **2010**, *5*, 487–496.
7. Stankovich, S.; Dikin, D. A.; Dommett, G. H. B.; Kohlhaas, K. M.; Zimney, E. J.; Stach, E. A.; Piner, R. D.; Nguyen, S. T.; Ruoff, R. S. Graphene-Based Composite Materials. *Nature* **2006**, *442*, 282–286.
8. Sato, K.; Noguchi, M.; Demachi, A.; Oki, N.; Endo, M. A Mechanism of Lithium Storage in Disordered Carbons. *Science* **1994**, *264*, 556–558.
9. Bizeto, M. A.; Shiguihara, A. L.; Constantino, V. R. L. Layered Niobate Nanosheets: Building Blocks for Advanced Materials Assembly. *J. Mater. Chem.* **2009**, *19*, 2512–2525.
10. Yoo, J. J.; Balakrishnan, K.; Huang, J.; Meunier, V.; Sumpter, B. G.; Srivastava, A.; Conway, M.; Mohana Reddy, A. L.; Yu, J.; Vajtai, R.; *et al.* Ultrathin Planar Graphene Supercapacitors. *Nano Lett.* **2011**, *11*, 1423–1427.
11. Yoon, Y.; Ganapathi, K.; Salahuddin, S. How Good Can Monolayer MoS₂ Transistors Be? *Nano Lett.* **2011**, *11*, 3768–3773.
12. Fowler, J. D.; Allen, M. J.; Tung, V. C.; Yang, Y.; Kaner, R. B.; Weiller, B. H. Practical Chemical Sensors from Chemically Derived Graphene. *ACS Nano* **2009**, *3*, 301–306.
13. Pacilé, D.; Meyer, J. C.; Girit, C. O.; Zettl, A. The Two-Dimensional Phase of Boron Nitride: Few-Atomic-Layer Sheets and Suspended Membranes. *Appl. Phys. Lett.* **2008**, *92*, 133107.
14. Joensen, P.; Frindt, R. F.; Morrison, S. R. Single-Layer MoS₂. *Mater. Res. Bull.* **1986**, *21*, 457–461.
15. Novoselov, K. S.; Jiang, D.; Schedin, F.; Booth, T. J.; Khotkevich, V. V.; Morozov, S. V.; Geim, A. K. Two-Dimensional Atomic Crystals. *Proc. Natl. Acad. Sci. U.S.A.* **2005**, *102*, 10451–10453.
16. Miremadi, B. K.; Morrison, S. R. The Intercalation and Exfoliation of Tungsten Disulfide. *J. Appl. Phys.* **1988**, *63*, 4970–4974.
17. Seo, J.-w.; Jun, Y.-w.; Park, S.-w.; Nah, H.; Moon, T.; Park, B.; Kim, J.-G.; Kim, Y. J.; Cheon, J. Two-Dimensional Nanosheet Crystals. *Angew. Chem., Int. Ed.* **2007**, *46*, 8828–8831.
18. Ma, R.; Sasaki, T. Nanosheets of Oxides and Hydroxides: Ultimate 2D Charge-Bearing Functional Crystallites. *Adv. Mater.* **2010**, *22*, 5082–5104.
19. Treacy, M. M. J.; Rice, S. B.; Jacobson, A. J.; Lewandowski, J. T. Electron Microscopy Study of Delamination in Dispersions of the Perovskite-Related Layered Phases K-[Ca₂Nb_{n-3}Nb_{3n-1}]: Evidence for Single-Layer Formation. *Chem. Mater.* **1990**, *2*, 279–286.
20. Takahashi, N.; Hata, H.; Kuroda, K. Exfoliation of Layered Silicates through Immobilization of Imidazolium Groups. *Chem. Mater.* **2010**, *23*, 266–273.
21. Naguib, M.; Kurtoglu, M.; Presser, V.; Lu, J.; Niu, J.; Heon, M.; Hultman, L.; Gogotsi, Y.; Barsoum, M. W. Two-Dimensional Nanocrystals Produced by Exfoliation of Ti₃AlC₂. *Adv. Mater.* **2011**, *23*, 4248–4253.
22. Barsoum, M. W. The M_{N+1}AX_N Phases: A New Class of Solids; Thermodynamically Stable Nanolaminates. *Prog. Solid State Chem.* **2000**, *28*, 201–281.
23. Barsoum, M. W.; Radovic, M. Mechanical Properties of the MAX Phases. In *Encyclopedia of Materials: Science and Technology*; Buschow, K. H. J., Cahn, R., Flemings, M., Ilshner, B., Kramer, E., Mahajan, S., Veysière, P., Eds.; Elsevier: Oxford, 2004; pp 1–16.
24. Wang, X. H.; Zhou, Y. C. Oxidation Behavior of Ti₃AlC₂ at 1000–1400 °C in Air. *Corros. Sci.* **2003**, *45*, 891–907.
25. Barsoum, M. W. Physical Properties of the MAX Phases. In *Encyclopedia of Materials: Science and Technology*; Buschow, K. H. J., Cahn, R., Flemings, M., Ilshner, B., Kramer, E., Mahajan, S., Veysière, P., Eds.; Elsevier: Oxford, 2006; pp 1–11.
26. Barsoum, M. W.; El-Raghy, T.; Farber, L.; Amer, M.; Christini, R.; Adams, A. The Topotaxial Transformation of Ti₃SiC₂ To Form a Partially Ordered Cubic TiC_{0.67} Phase by the Diffusion of Si into Molten Cryolite. *J. Electrochem. Soc.* **1999**, *146*, 3919–3923.
27. Naguib, M.; Presser, V.; Tallman, D.; Lu, J.; Hultman, L.; Gogotsi, Y.; Barsoum, M. W. On Topotactic Transformation of Ti₂AlC into a Ti-C-O-F Cubic Phase by Heating in Molten Lithium Fluoride in Air. *J. Am. Ceram. Soc.* **2011**, *94*, 4556–4561.
28. Barsoum, M. W.; Brodtkin, D.; El-Raghy, T. Layered Machinable Ceramics for High Temperature Applications. *Scr. Mater.* **1997**, *36*, 535–541.
29. Cullity, B. D. *Elements of X-ray Diffraction*; Addison-Wesley: Boston, MA, 1978.
30. Naguib, M.; Presser, V.; Lane, N.; Tallman, D.; Gogotsi, Y.; Lu, J.; Hultman, L.; Barsoum, M. W. Synthesis of a New Nanocrystalline Titanium Aluminum Fluoride Phase by Reaction of Ti₂AlC with Hydrofluoric Acid. *RSC Adv.* **2011**, *1*, 1493–1499.
31. Yoshida, A.; Hishiyama, Y.; Inagaki, M. Exfoliated Graphite from Various Intercalation Compounds. *Carbon* **1991**, *29*, 1227–1231.
32. Lv, W.; Tang, D.-M.; He, Y.-B.; You, C.-H.; Shi, Z.-Q.; Chen, X.-C.; Chen, C.-M.; Hou, P.-X.; Liu, C.; Yang, Q.-H. Low-Temperature Exfoliated Graphenes: Vacuum-Promoted Exfoliation and Electrochemical Energy Storage. *ACS Nano* **2009**, *3*, 3730–3736.
33. Makotchenko, V. G.; Grayfer, E. D.; Nazarov, A. S.; Kim, S.-J.; Fedorov, V. E. The Synthesis and Properties of Highly Exfoliated Graphites from Fluorinated Graphite Intercalation Compounds. *Carbon* **2011**, *49*, 3233–3241.
34. Du, Y. L.; Sun, Z. M.; Hashimoto, H.; Tian, W. B. First-Principles Study of Polymorphism in Ta₄AlC₃. *Solid State Commun.* **2008**, *145*, 461–464.
35. McAllister, M. J.; Li, J.-L.; Adamson, D. H.; Schniepp, H. C.; Abdala, A. A.; Liu, J.; Herrera-Alonso, M.; Milius, D. L.; Car, R.; Prud'homme, R. K.; *et al.* Single Sheet Functionalized Graphene by Oxidation and Thermal Expansion of Graphite. *Chem. Mater.* **2007**, *19*, 4396–4404.
36. Wang, X.; Tabakman, S. M.; Dai, H. Atomic Layer Deposition of Metal Oxides on Pristine and Functionalized Graphene. *J. Am. Chem. Soc.* **2008**, *130*, 8152–8153.
37. Xiao, J.; Mei, D.; Li, X.; Xu, W.; Wang, D.; Graff, G. L.; Bennett, W. D.; Nie, Z.; Saraf, L. V.; Aksay, I. A.; *et al.* Hierarchically Porous Graphene as a Lithium–Air Battery Electrode. *Nano Lett.* **2011**, *11*, 5071–5078.
38. Eklund, P.; Palmquist, J. P.; Höwing, J.; Trinh, D. H.; El-Raghy, T.; Högberg, H.; Hultman, L. Ta₄AlC₃: Phase Determination, Polymorphism and Deformation. *Acta Mater.* **2007**, *55*, 4723–4729.
39. Salama, I.; El-Raghy, T.; Barsoum, M. W. Synthesis and Mechanical Properties of Nb₂AlC and (Ti,Nb)₂AlC. *J. Alloys Compd.* **2002**, *347*, 271–278.
40. Zhou, Y.; Meng, F.; Zhang, J. New MAX-Phase Compounds in the V–Cr–Al–C System. *J. Am. Ceram. Soc.* **2008**, *91*, 1357–1360.
41. Li, X.; Zhu, Y.; Cai, W.; Borysiak, M.; Han, B.; Chen, D.; Piner, R. D.; Colombo, L.; Ruoff, R. S. Transfer of Large-Area Graphene Films for High-Performance Transparent Conductive Electrodes. *Nano Lett.* **2009**, *9*, 4359–4363.
42. Blake, P.; Brimicombe, P. D.; Nair, R. R.; Booth, T. J.; Jiang, D.; Schedin, F.; Ponomarenko, L. A.; Morozov, S. V.; Gleeson, H. F.; Hill, E. W.; *et al.* Graphene-Based Liquid Crystal Device. *Nano Lett.* **2008**, *8*, 1704–1708.
43. Rafiee, J.; Rafiee, M. A.; Yu, Z.-Z.; Koratkar, N. Superhydrophobic to Superhydrophilic Wetting Control in Graphene Films. *Adv. Mater.* **2010**, *22*, 2151–2154.
44. Gogotsi, Y. Controlling Graphene Properties through Chemistry. *J. Phys. Chem. Lett.* **2011**, *2*, 2509–2510.
45. Naguib, M.; Come, J.; Dyatkin, B.; Presser, V.; Taberna, P.-L.; Simon, P.; Barsoum, M. W.; Gogotsi, Y. MXene: A Promising Transition Metal Carbide Anode for Lithium-Ion Batteries. *Electrochem. Commun.* **2012**, *16*, 61–64.